Research Square

Preprints are preliminary reports that have not undergone peer review.
They should not be considered conclusive, used to inform clinical practice,
or referenced by the media as validated information.

Research on signal reconstruction of ground-penetrating radar based on matrix pencil method

Yanan Li
Guilin University of Technology
Kang He
Shen Zhen Power Supply Planning Design Institute Co.,LTD
Yuexing Yu
The fifth Geological Brigade of Jiangxi Geological Bureau
Runlin Luo
luorunlin@glut.edu.cn
Guilin University of Technology
Changwei Li
Guilin University of Technology
Guozhi Tang
Guangxi Nonferrous Survey&Design Institute

Article

Keywords: Ground-penetrating Radar, Denoising, Matrix Pencil method, Signal reconstruction

Posted Date: November 5th, 2026

DOI: https://doi.org/10.21203/rs.3.rs-11399204/v1

License: This work is licensed under a Creative Commons Attribution 4.0 International License.
Read Full License

Additional Declarations: No competing interests reported.

Research on signal reconstruction of ground-penetrating radar based on matrix pencil method

Yanan Li[ab], Kang He[c], Yuexing Yu[d], Runlin Luo[a]* , Changwei Li[a], Guozhi Tang[e]

[a] *College of Earth Sciences*, *Guilin University of Technology*, *Guilin 641004,China*
[b] *Key Laboratory of Geophysical Electromagnetic Probing Technology of Ministry of Natural Resource of the People's Republic of China, Langfang,065000,China*
[c]*Shen Zhen Power Supply Planning Design Institute Co.,LTD*, *Shenzhen 518066,China*
[d] *The fifth Geological Brigade of Jiangxi Geological Bureau, Xinyu 338000, China*
[e] *Guangxi Nonferrous Survey&Design Institute*, *Nanning 530031*,*China*

Abstract

Ground-penetrating radar (GPR) signals are often severely contaminated by random noise, which weakens deep or small-target reflections and reduces interpretability. This paper proposes a GPR signal reconstruction method based on the matrix pencil (MP) method. The GPR trace is modeled as a sum of damped complex exponentials and reconstructs the effective signal by estimating key parameters, including the number of dominant poles, pole values, and residues, through singular value decomposition and least-squares fitting. The optimal number of dominant poles is determined to balance noise suppression and signal fidelity. The proposed method is validated using synthetic data with different signal-to-noise ratios, laboratory physical-model data from a buried metal pipe, and field data from a full-scale shield tunnel grouting test platform. Quantitative evaluations using peak signal-to-noise ratio and image entropy demonstrate that the MP method significantly suppresses high-frequency random noise, preserves subtle reflection features, and improves image clarity. Both synthetic and real-data results confirm that the MP method outperforms conventional denoising techniques in enhancing GPR data interpretability, offering a practical and effective tool for underground defect detection and engineering quality inspection.

Keywords: Ground-penetrating Radar; Denoising; Matrix Pencil method; Signal reconstruction

1. Introduction

Ground-penetrating radar (GPR) is an important geophysical tool for investigating the shallow subsurface [1]. As a non-invasive and non-destructive method, it can be used to detect landmines, cables, pipes, reinforcement bars, fractures in bedrock, subsurface cavities, sediment, and moisture [2]. Because of the large bandwidth of GPR systems [3], GPR signals are usually contaminated by various types of noise, such as ringing noise [4], sferics noise [5], and random noise. When GPR data are contaminated by noise, reflections from deep interfaces become extremely weak, reducing the target-identification capability of GPR. Therefore, noise elimination is crucial for enhancing GPR detection performance [6].

Recently, many methods have been proposed for GPR signal denoising. Spatial-domain filtering is a traditional approach, including median filtering [7] and total variation denoising [8]. Transforming raw data into different domains is also common in GPR data processing. For example, converting GPR data

*Corresponding author:Runlin Luo, luorunlin@glut.edu.cn
E_mail addresses:lyn2008@glut.edu.cn(Y.Li),2352521827@qq.com (K. He),yuyuexing0@163.com(Y.Y), luorunlin@glut.edu.cn(R. Luo), lcw@glut.edu.cn(C. Li),944080762@qq.com(G. Tang)

into the frequency domain using the Fourier transform allows useful signals to be retained while noise is removed based on their differing spectral characteristics [9-11]. Principal component analysis (PCA) preserves highly correlated signal components while discarding uncorrelated noise, thereby achieving denoising [12-14]. However, PCA is limited in noise removal, particularly for correlated noise in GPR data [15,16], and its performance may degrade when processing localized signals [17]. Because both GPR and seismic methods rely on wave propagation and interaction with subsurface media to extract structural information, some noise-reduction techniques from seismic data processing have been adopted for GPR, such as muting, median filtering, and F-K (or F-X) filtering [18,19]. Although these methods perform well in removing stable noise and noise with frequency bands distinct from the signal, they can cause signal distortion and introduce false anomalies when signal and noise spectra overlap. In recent years, advances in computational hardware and algorithms have driven rapid progress in artificial intelligence, especially deep learning based on neural networks. For GPR denoising, researchers have constructed neural-network models that remove random noise from GPR data through backpropagation algorithms and have achieved promising results [20-21].

For GPR image denoising, innovative mathematical techniques have been introduced, such as the windowed Fourier transform, independent component analysis (ICA), the Hilbert transform, and the Hilbert-Huang transform [22-24]. The advancement of complex signal processing has also highlighted the potential of empirical mode decomposition (EMD) and related methods for improving GPR data interpretation. However, these methods face challenges such as limited theoretical foundations and mode mixing [25,26]. The Hilbert transform, with its multidirectional and adaptive characteristics, has been widely applied to denoising non-stationary signals in GPR data, although its practical effectiveness remains insufficiently validated [27,28]. Singular spectrum analysis (SSA) processes GPR data through singular value decomposition (SVD), separating effective signals and interference based on singular spectra and eigenvectors. By reconstructing data using low-order eigenvectors that represent high variance and differ from noise, SSA achieves spatial denoising and improves the signal-to-noise ratio [29,30]. To address the limitations of traditional PCA in clutter suppression, wavelet transform has been combined with PCA. This hybrid method integrates subspace projection and adaptive transverse filtering, improving clutter suppression and radar signal processing accuracy. Techniques such as wavelet transform, PCA, and adaptive filtering complement one another and demonstrate excellent performance in increasing the signal-to-noise ratio and enhancing image clarity [31,32]. Traditional Hilbert transform methods are highly sensitive to threshold settings; combining the Hilbert transform with SVD enhances GPR noise suppression by simultaneously removing random noise and amplifying reflection signals. This approach identifies and separates noise from effective signals using SVD and then enhances the signal through the Hilbert transform, improving data quality and interpretive accuracy [33,34]. To address high-density noise in GPR images caused by geological or environmental factors, which obscures effective signals and renders data unreadable, a novel denoising method, PM-NRM, has been proposed. By integrating the PM algorithm with a noise recognition model, this method uses partial differential equations to identify noise points based on the contrast between noise and background values, achieving denoising through an iterative conditional mode algorithm [35]. Furthermore, Wang et al. proposed a solution to the instability of training generative adversarial networks (GANs) for GPR image generation [36]. By incorporating a gradient penalty with Wasserstein distance, they generated GPR images and constructed GPR datasets using time-domain finite-difference simulation and real field-acquired images, significantly improving GPR image denoising performance.

Since its introduction in the mid-1980s, wavelet transform analysis has developed rapidly and become a widely used tool in signal processing, image processing, and data analysis. Unlike the Fourier transform, which analyzes signals solely in the frequency domain, the wavelet transform enables simultaneous time-frequency analysis, making it particularly effective for non-stationary signals. The inherent

"focusing" ability of the wavelet transform allows fine-grained signal analysis and processing at multiple scales, leading to enhanced clarity in signal details. This multiresolution capability has demonstrated superior efficiency and effectiveness in various applications, including GPR data denoising and analysis [37]. The concept of wavelet-based data denoising was first proposed by Mallat [38]. Although widely applied, wavelet transform faces challenges such as fixed basis selection, which may not suit all data types or applications, and suboptimal performance with high-dimensional data because of increased computational complexity. In addition, threshold determination remains critical and often relies on empirical knowledge and trial-and-error experiments, which can yield varying results depending on the selected threshold [39]. To overcome these limitations, wavelet transform is often combined with other algorithms for more effective clutter and noise reduction in GPR data. This hybrid approach leverages the time-frequency localization of wavelet transform while applying complementary denoising techniques. However, a notable risk is the potential distortion or loss of hyperbolic reflection signals, because complex signals or overlapping frequency components may cause valid signals to be misclassified as noise. Thus, careful algorithm selection and optimization are crucial to preserving signal integrity during noise reduction [40-42]. For non-stationary signal denoising, multiresolution and adaptive threshold methods, including wavelet and curvelet transforms, have been widely applied to GPR data with promising results and demonstrate practicality in real-world GPR data processing [15].

In electromagnetic problems, signal models in the form of sums of exponentially decaying terms-known as the "sum of exponential decay" model-are commonly employed to extract features such as signal poles. This model effectively reflects signal amplitude, phase, and poles, and has been widely applied in fields such as geophysical exploration and communications for estimating characteristic parameters such as poles and residues [43]. The least-squares matrix pencil method, which adopts the sum of damped exponentials model, eliminates the influence of harmonics and decaying DC components. Comparisons with Fourier-based methods have demonstrated its high accuracy [44]. Matrix pencil (MP) algorithms have also been used for direction-of-arrival (DOA) estimation in radar, achieving improved accuracy and reduced computational complexity compared with total least-squares ESPRIT algorithms [45]. In addition, researchers have applied the MP method to time-domain airborne electromagnetic [46] and transient electromagnetic data processing [47]. The MP method can simplify the algorithm and improve computational efficiency when denoising electromagnetic data.

In this paper, the MP is applied to denoise GPR signals.This approach seeks to improve the signal-to-noise ratio (SNR), enhance resolution, and preserve image details. In doing so, it is expected to significantly improve the accuracy and effectiveness of GPR image interpretation.

2. Theory of GPR signal reconstruction based on MP

In electromagnetic problems, to extract the pole information of a signal, the sampled data is often represented as a sum of a series of complex exponential signals, referred to as the "sum of complex exponentials " signal model [48]. The electromagnetic wave signals received by the GPR antenna exhibit the same form as the "sum of damped exponentials" signal model and can be expressed as:

$$y(t) = x(t) + n(t), \tag{1}$$

$$x(t) \approx \sum_{i=1}^{M} R_i e^{s_i t}, \tag{2}$$

where $y(t)$ represents the observed GPR signal data, $x(t)$ denotes the effective signal, R_i is the residue, and $S_i=\alpha_i+\mathrm{i}\omega_i$, where αi is the damping factor and $\omega_i=2\pi f_i$ is the angular frequency. M refers to the number of main poles, and $n(t)$ represents the mixed noise.

Rewrite Equation (2) as:

$$x(t) \approx \sum_{i=1}^{M} R_i z_i \quad , \tag{3}$$

where

$$z_i = e^{s_i t} , \tag{4}$$

z_i is the ith pole.

For noise-contaminated GPR signal ($n(t)\neq 0$), the N data points of $y(t)$ are constructed into a matrix $[Y]$ of dimensions $(N\text{-}L)\times(L+1)$,defined as follows:

$$[Y] = \begin{bmatrix} y(0) & y(1) & \cdots & y(L) \\ y(1) & y(2) & \cdots & y(L+1) \\ \vdots & \vdots & \ddots & \vdots \\ y(N-L-1) & y(N-L) & \cdots & y(N-1) \end{bmatrix}_{(N-L)\times(L+1)} . \tag{5}$$

The matrix $[Y]$ can be decomposed into two $(N\text{-}L)\times L$ matrices, denoted as $[Y_1]$ and $[Y_2]$, where removing the last column from $[Y]$ results in $[Y_1]$, and removing the first column from $[Y]$ results in$[Y_2]$, L is pencil parameter.

$$[Y_1] = \begin{bmatrix} \mathrm{y}(0) & y(1) & \cdots & y(L-1) \\ y(1) & y(2) & \cdots & y(L) \\ \vdots & \vdots & \ddots & \vdots \\ y(N-L-1) & y(N-L) & \cdots & y(N-2) \end{bmatrix}_{(N-L)\times L} , \tag{6}$$

$$[Y_2] = \begin{bmatrix} y(1) & y(2) & \cdots & y(L) \\ y(2) & y(3) & \cdots & y(L+1) \\ \vdots & \vdots & \ddots & \vdots \\ y(N-L) & y(N-L+1) & \cdots & y(N-1) \end{bmatrix}_{(N-L)\times L} . \tag{7}$$

L plays a crucial role in eliminating data noise, with its value typically ranging between $N/3$ and $N/2$. After multiple tests, it was found that the error is minimized when $L= N/2$.

The matrix $[Y]$ is then subjected to SVD:

$$[Y] = [U][\Sigma][V]^H , \tag{8}$$

where $[U]$ and $[V]$ are unitary matrices, composed of the eigenvectors of $[Y][Y]^H$ and $[Y]^H[Y]$, respectively. H denotes the conjugate transpose of matrix. $[\Sigma]$ is the diagonal matrix consisting of the singular values of $[Y]$. By performing the transformation on equation (7), we obtain:

$$[U]^H [Y][V] = [\Sigma] \quad . \tag{9}$$

After performing SVD, the singular values in the diagonal matrix $[\Sigma]$ are arranged in descending order. A ratio is then calculated between the singular values and the largest singular value. The way to evaluate M is as follows.

For a singular value σ_c, it is considered significant if it satisfies:

$$\sigma_{\mathrm{c}} / \sigma_{\max} \approx 10^{-p} \quad , \tag{10}$$

where p represents the precision level, and σ_c is the critical singular value (the M-th singular value). Typically, it is considered that the singular values beyond M are significantly affected by noise, they are set to be 0.

Once the M is determined, $[V^*]$, which contains only M dominant right-singular vectors of $[V]$ is then constructed.

$$\left[V^*\right]=\left[v_1, v_2, \ldots v_M\right]. \tag{11}$$

By discarding the portion of the right singular vectors corresponding to the singular values from M+1 to L, we obtain:

$$[Y_1]=[U]\left[\Sigma^*\right]\left[V_1^*\right]^H, \tag{12}$$

$$[Y_2]=[U]\left[\Sigma^*\right]\left[V_2^*\right]^H. \tag{13}$$

where $[V_1^*]$ is obtained by removing the last row of $[V^*]$, and $[V_2^*]$ is obtained by removing the first row of $[V^*]$. $[\Sigma^*]$ is composed of the M singular values corresponding to the values that meet the precision requirement from$[\Sigma]$.

Then define matrix pencil:

$$[Y_2]-\lambda[Y_1]=[Z_1][R]\left([Z_0]-\lambda I\right)[Z_2], \tag{14}$$

where λ is a scalar variable.

$$[Z_0]=diag\left[z_1, z_2, \cdots, z_M\right], \tag{15}$$

$$[R]=diag\left[R_1, R_2, \cdots, R_M\right], \tag{16}$$

$$[Z_1]=\begin{bmatrix} 1 & 1 & \cdots & 1 \\ z_1 & z_2 & \cdots & z_M \\ \vdots & \vdots & \ddots & \vdots \\ z_1^{(N-L-1)} & z_2^{(N-L-1)} & \cdots & z_M^{(N-L-1)} \end{bmatrix}, \tag{17}$$

$$[Z_2]=\begin{bmatrix} 1 & 1 & \cdots & z_1^{L-1} \\ 1 & z_2 & \cdots & z_2^{L-1} \\ \vdots & \vdots & \ddots & \vdots \\ 1 & z_M & \cdots & z_M^{(L-1)} \end{bmatrix}. \tag{18}$$

The signal poles z_is are the generalized eigenvalue of $[Y_2]$-λ$[Y_1]$, so z_is can be solved by calculating the eigenvalue of the matrix of $[C]$ as follow:

$$[C]=\left([Y_1]^H[Y_1]\right)^{-1}[Y_1]^H[Y_2]. \tag{19}$$

After obtaining M and z_is, the residues R_is can be determined from Eq.13 by the least squares method.

$$\begin{bmatrix} y_0 \\ y_1 \\ \vdots \\ y_{N-1} \end{bmatrix}=\begin{bmatrix} 1 & 1 & \cdots & 1 \\ z_1 & z_2 & \cdots & z_M \\ \vdots & \vdots & \ddots & \vdots \\ z_1^{N-1} & z_2^{N-1} & \cdots & z_M^{N-1} \end{bmatrix}\bullet\begin{bmatrix} R_1 \\ R_2 \\ \vdots \\ R_M \end{bmatrix}. \tag{20}$$

Once the parameters M, R_is, and z_is are determined, the GPR signal can be reconstructed using Equation (3).

3.Examples

3.1. Synthetic data

To verify the feasibility of the matrix pencil method for GPR signal processing, a model containing a single 0.7 m × 0.7 m square cavity was established (Fig. 1a). The cavity, with a central depth of 1.85 m, is embedded in limestone overlaid by a 1.0 m-thick clay layer. The cavity is filled with a mixture of air, water and mud. The medium parameters are listed in Table 1. GPR signals were simulated using the open-source software gprMax [49]. A Perfectly Matched Layer (PML) boundary condition was adopted in this model. The excitation source was a Ricker wavelet with a central frequency of 200 MHz. The grid size was set to $\Delta x = \Delta y = 0.01$m, and the time window was set to 125ns. The antenna moved with a step interval of 0.05 m, and a total of 87 traces were acquired. Point A at the x-coordinate of 2.5m was selected to verify the effectiveness of the MP method.

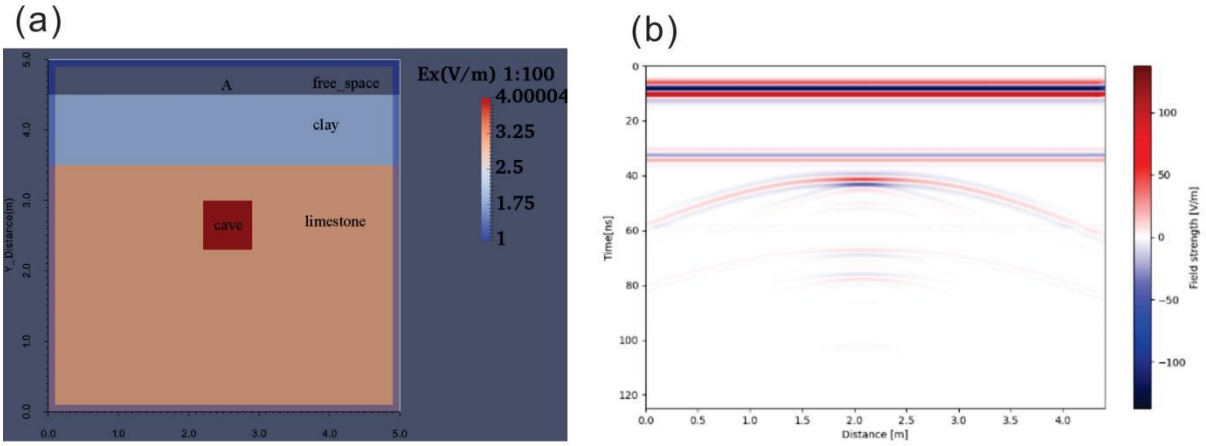


Figure 1. (a) The cavity model and (b) synthetic GPR responses with noise-free

Table 1. Parameters of synthetic model

media	relative dielectric constant	conductivi-ty/(s.m-1)	relative permea-bility	velocity of electromagnetic wave(/m.ns-1)
limestome	7	10-9	1	0.11
cavity	30	0.5	1	0.07
clay	10	0.2	1	0.06

The GPR responses are illustrated in Fig. 1b. The reflection signals from the top of the cavity and the clay-limestone interface are distinct. Two different levels of white noise were injected into the simulated GPR signals, with the corresponding *SNR*s set to 5 dB and 10 dB (Fig. 2).The mathematical definition of SNR is given in Equation(21). As an *SNR* of 5 dB, the cavity reflection is extremely weak. At an *SNR* of 10 dB, the target signal becomes prominent, accompanied by considerable background noise.

$$SNR = 10\lg(\frac{P_S}{P_N}) \quad , \tag{21}$$

where P_S and P_N represent the power of the signal and noise, respectively, and *SNR* is the signal-to-noise Ratio.

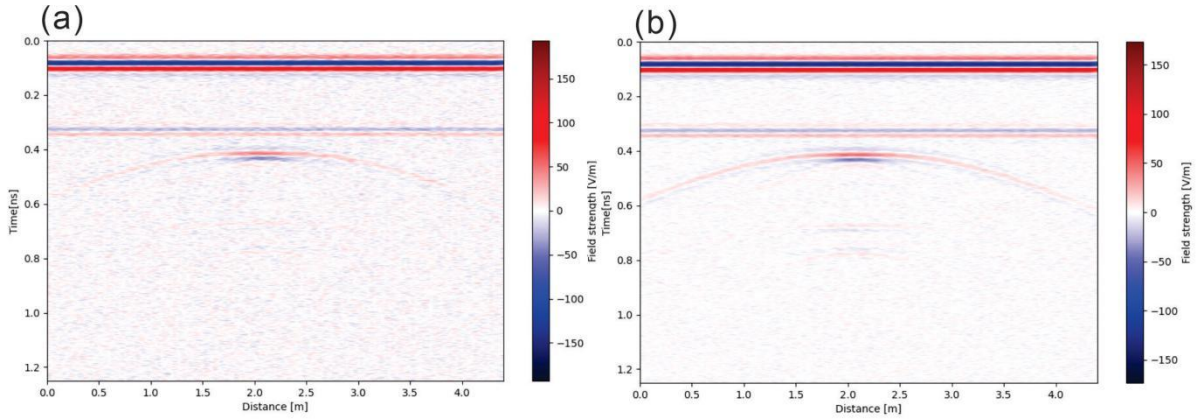


Figure 2 GPR responses with noise of the synthetic model,(a) SNR=5dB,(b)SNR=10dB

We selected the waveform trace at Point A (Trace A, see Fig. 1a) to analyze the influence of the number of dominant poles (M). As shown in Fig. 3, for signals with SNRs of 5 dB and 10 dB, the reflection signals from the cavity top and the clay-limestone interface are nearly indistinguishable. The reflection signal remains weak at an SNR of 20 dB and becomes distinct at 30 dB. The GPR signals were then reconstructed using the MP method with M set to 18, 28, 30, 32, 34, and 36. The results indicate that when M takes an appropriate value, the reconstructed signals show clearer target reflection features and achieve effective noise suppression. In contrast, an excessively large or small M causes severe oscillation in the reconstructed signals, as typified by the traces at SNR = 5 dB (M = 36) and SNR = 30 dB (M = 18).

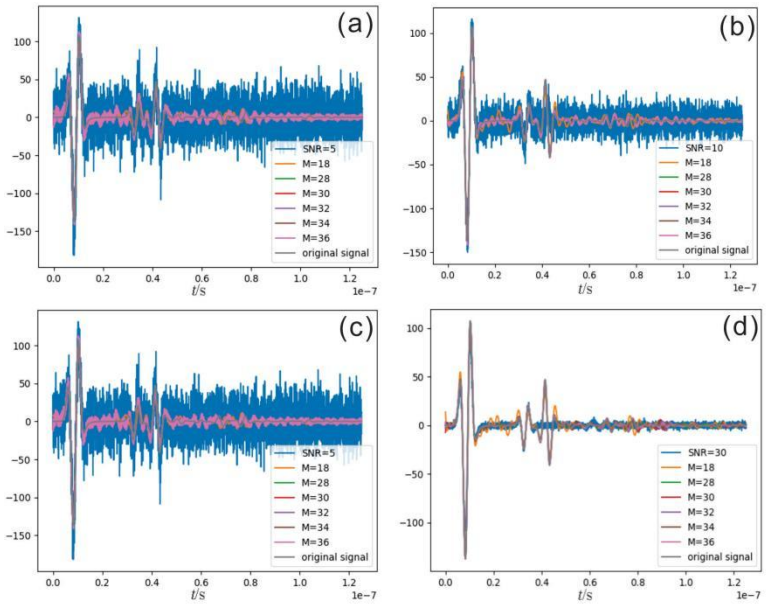


Figure 3 Signal of Trace A contaminated white noise with (a)SNR=5dB,(b)SNR=10dB,(c)SNR=20dB,(d)SNR=30dB

The root mean square error (*RMSE*, Eq.22) is used to describe the effectiveness of the denoising process. The noise is lower, *RMSE* is smaller.

$$RMSE = \left[\frac{1}{N} \sum_{n=1}^{N} \left| y(n) - y_m(n) \right|^2 \right]^{1/2}, \qquad (22)$$

where $y(n)$ is the reconstructed data and $y_m(n)$ is the synthetic data with noise free.

Figure 4 illustrates the RMSE and SNR of the reconstructed GPR waveform from Point A for different M values, where the original signal has an SNR of 5 dB. As shown in Fig. 4, the maximum SNR is 37.4 and the minimum RMSE is 0.5022 when M = 32, at which the reconstructed signal achieves its

closest match to the noise-free signal in this model. Because M is determined by the parameter p in Eq. (10), optimal GPR signal reconstruction can be pursued by testing different p values.

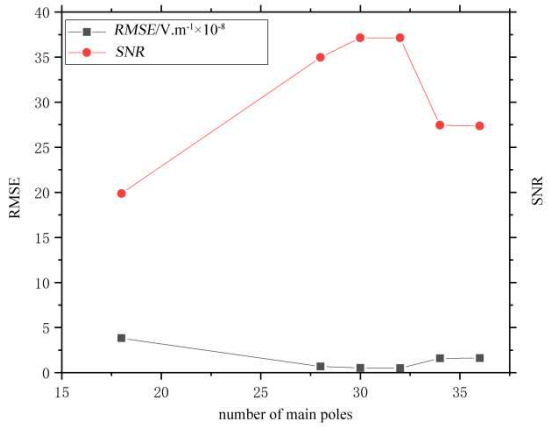


Figure 4 The curves of RMSE and SNR VS M

For B-scan GPR images, the peak signal-to-noise ratio (*PSNR*) and entropy value(*Q*) are used to evaluate the denoising performance of MP.

$$PSNR = 20\log_{10}\left[\frac{\max(s)}{MSE}\right], \tag{23}$$

$$MSE = \frac{1}{nm}\sum_{i=1}^{n}\sum_{j=1}^{m}\left[X_{i,j} - X'_{i,j}\right]^2, \tag{24}$$

where n is number of GPR traces and m is time samples, and $X(i,j)$ and $X'(i,j)$ are the original signal and denoised signal for the i-th trace and the j-th time sample respectively, max(s) is the peak value of de-noised signal.

PSNR quantifies the ratio between effective signal and noise. Higher *PSNR* values indicate lower noise levels and a greater proportion of effective signals within the data, thereby enhancing data interpretation. Image entropy(*Q*) is used to describe the degree of disorder in an image. For denoised GPR images, a higher entropy value indicates a more chaotic image, while a lower entropy value suggests a clearer image with more defined target signals.

$$Q = \frac{(\sum_{i=1}^{m}\sum_{j=1}^{n}X_{i,j}^2)^2}{\sum_{i=1}^{m}\sum_{j=1}^{n}X_{i,j}^4}, \tag{25}$$

where m is the number of GPR traces, and n is time samples.

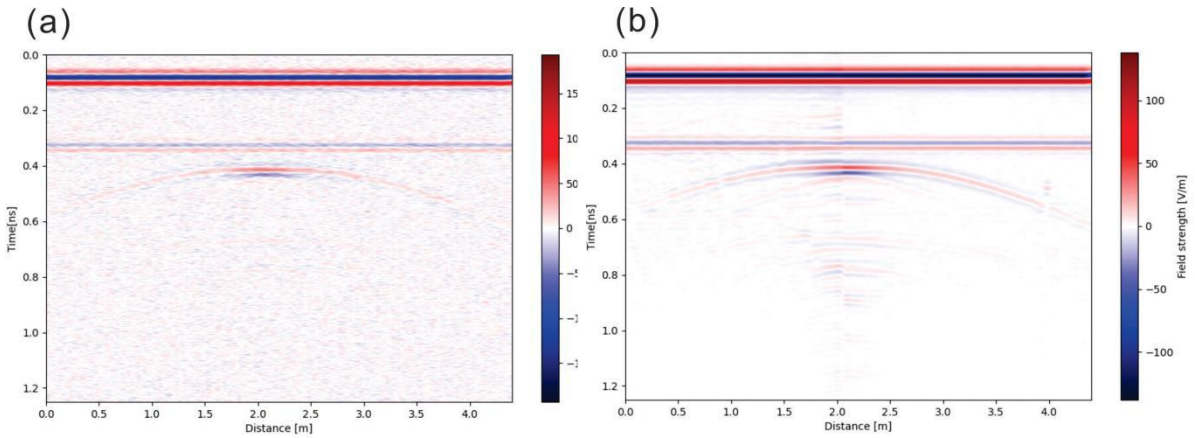


Figure 5. GPR B-scan images of synthetic model,(a) original signal with SNR=5dB,(b) reconstructed B-scan image

Figure5 shows the original image with SNR=5dB and the reconstructed image with M=32. In the original image, the white noise is obvious and the reflection of the cavity is ambiguous. While in the reconstructed image, the white noise has been significantly suppressed and the cavity interface reflection pattern exhibits a well-defined event. Q of is the reconstructed signal 2.757 ,which almost the same as the Q of signal with noisy-free. The PSNR has increased from 34.567dB to 37.883dB (see Tab.2). The MP method effectively improved PSNR and reduced the entropy values of the target images.

Table 2. *Q* and *PSNR* of synthetic data

	Q	*PSNR*/dB
Noisy-free GPR signal	2.710	--
GPR signal with SNR=5	3.530	34.567
Reconstructed GPR signal	2.757	37.883

3.2. Experimental data

A physical simulation experiment was conducted in the laboratory using a sandpit model filled with quartz sand. The sandpit dimensions were 4.5 m × 3.0 m × 1.1 m. In the middle of the sandpit, a 1.1 m long metal pipe was buried at a depth of 0.2 m. The left end of the pipe was 1.15 m from the sandpit boundary, and the right end was 1.35 m from the boundary. The placement of the metal pipe and the layout of the survey lines are shown in Fig. 6. The survey line was 2.3 m long and intersected the central pipe perpendicularly at the 1.15 m position.

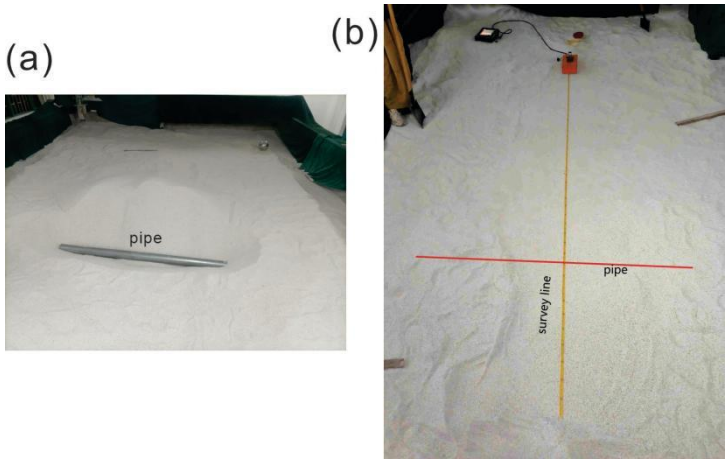


Figure 6 Experimental scene(a) metal pipe,(b) survey line

In this physical experiment, we employed the GSSI SIR-4000 ground penetrating radar system with a 400 MHz antenna. The antenna was scanned along the prearranged survey line. As illustrated in Figure 7a, the hyperbolic reflection signals generated by the metal pipe became distorted due to white noise and attenuation.

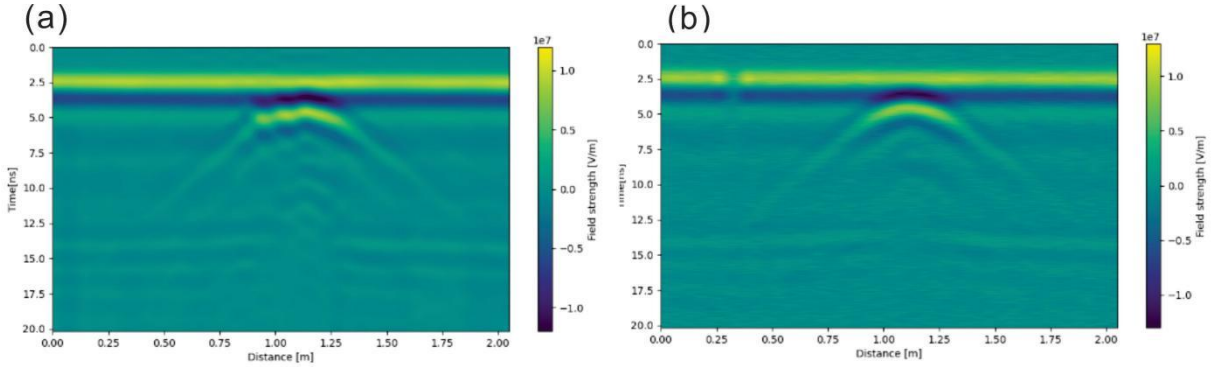


Figure 7 GPR images of experimental model,(a) original B-scan image,(b) reconstructed B-scan image

The MP method was applied to the experimental data, and the result is shown in Fig. 7b. The white noise is partially removed and the quality of the GPR image is effectively improved. The reconstructed signal is greatly enhanced: the B-scan image becomes clear and the hyperbolic signal shows good continuity. The *PSNR* of the reconstructed signal reaches 36.554 dB, an increase of 55.9% compared with the original value of 23.576 dB. The reconstruction quality factor *Q* is 3.239, a decrease of 22.5% relative to the original signal (Table 3).

Table 3. Q and PSNR of experimental data

	PSNR/dB	*Q*
Original signal	23.576	4.182
Reconstructed signal	36.554	3.239

Figure 8 presents a comparison of the reconstruction results for Trace 23 at the 1.15 m position and Trace 30 at the 1.5 m position. The reconstructed signals show excellent agreement with the original data: the peak and trough locations of the primary reflections, as well as the overall waveform trends, are closely matched, indicating that the key reflection features are fully preserved. Meanwhile, high-frequency random noise present in the original signals is effectively suppressed after reconstruction, resulting in smoother waveforms and a substantial improvement in the overall signal-to-noise ratio.

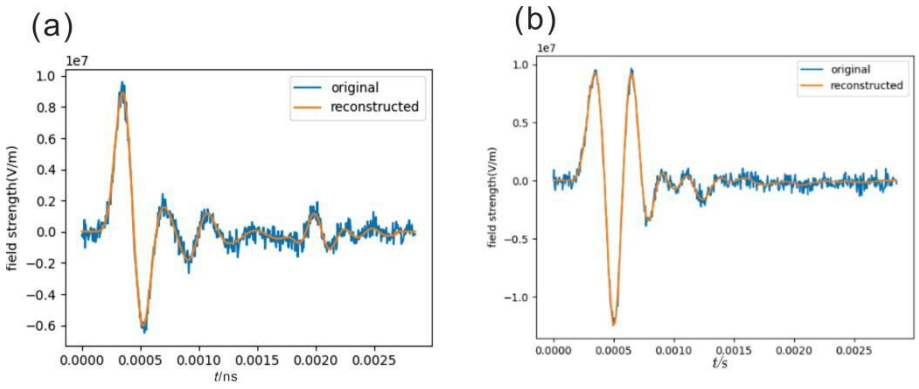


Figure 8. GPR signal before and after denoised at (a) 23rd trace,(b) 30th trace

3.3 Field data

The quality of backfill grouting behind tunnel segments exerts a decisive influence on the safety of shield excavation and the stability of adjacent structures. Insufficient grout compaction, uneven grout distribution or grout voids can trigger deformation in surrounding rock and soil, which may further result in ground subsidence, building cracks and other geotechnical hazards. Hence, rapid and accurate inspection of grouting quality is of great practical significance. To develop reliable detection approaches, the Guangxi Nonferrous Exploration and Design Research Institute built a full-scale test platform (Fig.9) to simulate shield tunnel segment rings [50,51].

This test platform is built to simulate a standard tunnel segment ring. The precast segments are assembled circumferentially and connected by bolts, with an outer diameter of 6.0 m, an inner diameter of 5.4 m and a segment thickness of 0.3 m. An annular gap of 20-35 cm behind the segments was designed to mimic the cavities generated during shield tunnelling. To simulate grouting voids, PVC pipes with outer diameters of 5 cm, 10 cm and 16 cm (all 165 cm in length) were vertically embedded in the grout layer, as illustrated in Fig.9b. All artificial defects are numbered sequentially from 1 to 12 in a clockwise

direction. Defect No. 2 is created by excavating a 25 cm-wide zone on the outer side of the segment ring and backfilling it with gravel and water, simulating insufficient grouting and local void collapse.

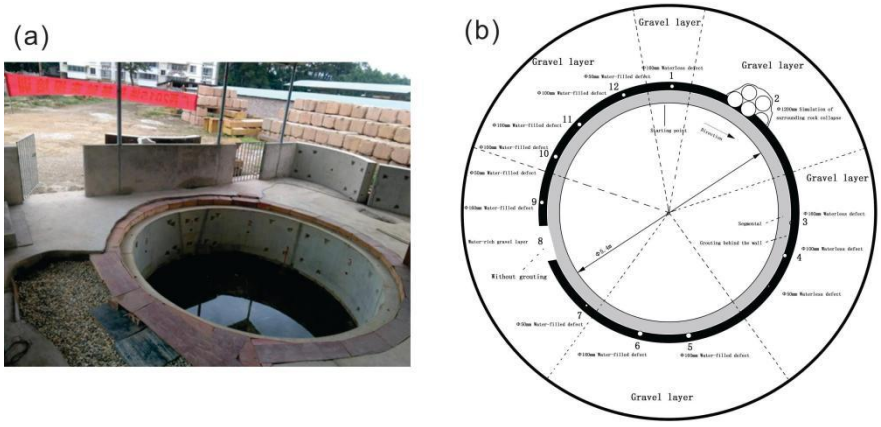


Figure 9. Schematic plan of defect structures on the experimental platform (a)photo of experimental platform, (b)Schematic plan of defect structures

To verify the applicability of ground-penetrating radar (GPR) in grouting quality inspection, a GPR survey line was arranged clockwise along the inner wall of the segment ring. The survey line starts roughly 30 cm counterclockwise from Defect No. 1 (Fig. 9b), spanning 17.15 m with partial overlap at both ends. Data collection was carried out using a GSSI SIR-4000 GPR system equipped with a 900 MHz antenna. The trace interval was set to 2 cm and the sampling time window to 32 ns. Figure 10a presents distinct reflection signals from the segment-grout interface and segment joints. Nevertheless, most defect signatures are masked by background noise, and only faint responses can be observed from Defects No. 2 and No. 11.

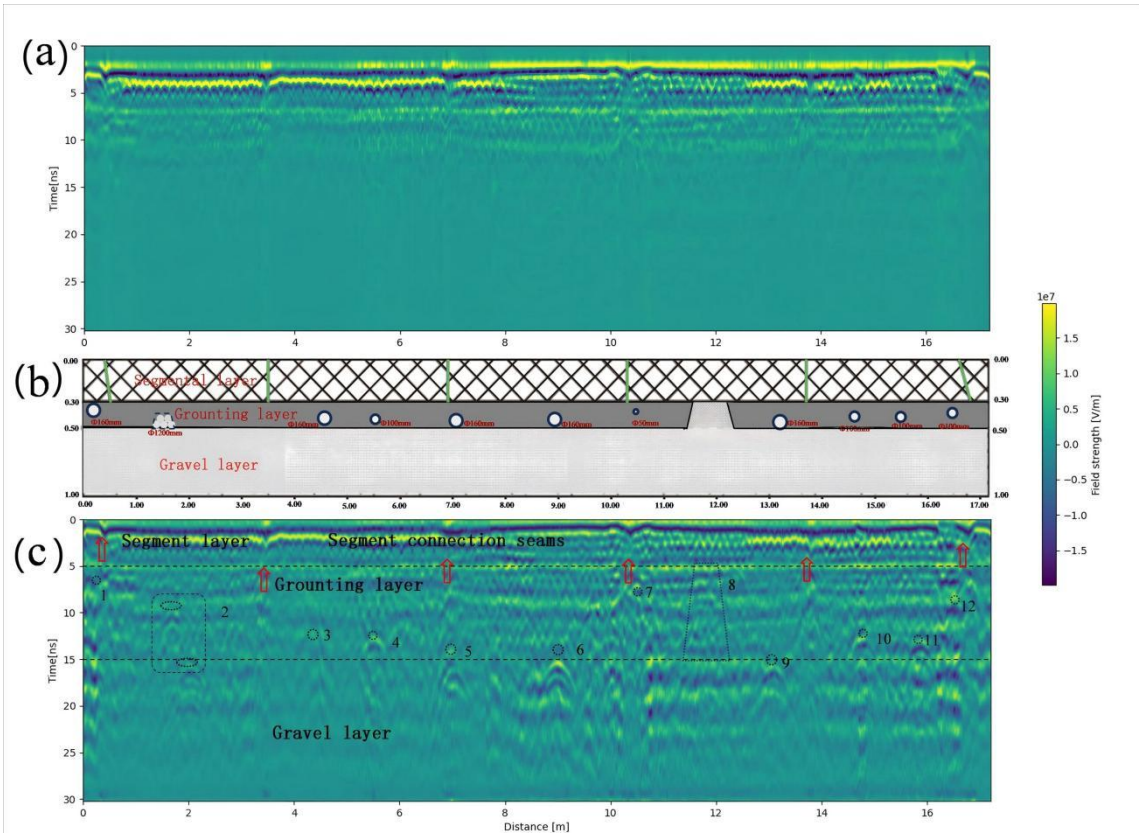


Figure 10. Field results (a) raw GPR signal, (b) profile of the experimental platform, (c) reconstructed signal

After applying the MP algorithm, random noise was effectively eliminated and the image resolution was greatly improved (Fig. 10c). Defects adjacent to segment joints, including No. 1, No. 7, and No. 12, show subtle anomalies, while other defects become clearly identifiable. Due to electromagnetic wave scattering, the anomalous area of Defect No. 2 appears enlarged. As summarized in Table 4, MP processing increases the peak signal-to-noise ratio (PSNR) and decreases image entropy, fully validating the favorable denoising performance of the proposed method. Single-trace analysis (Fig. 11) further shows that high-frequency noise is well suppressed and the reconstructed waveforms become much smoother.

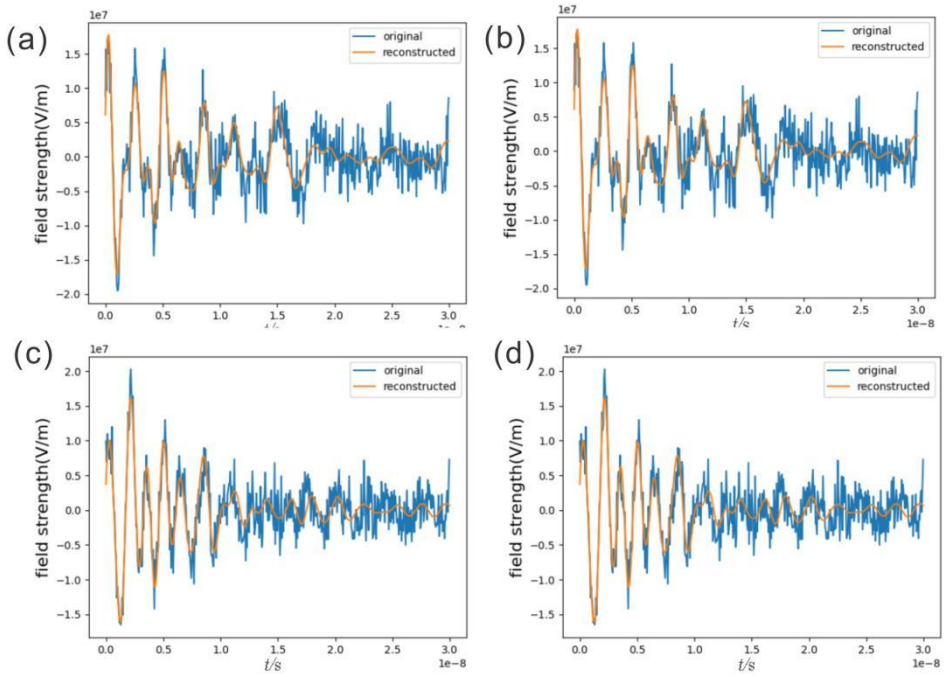


Figure 11 GPR Trace before and after denoised at (a) 2.7m-mark,(b) 7.3m-mark,(c)9.3m-mark,(d)12m-mark

Table 4. PSNR and Q of field data

	PSNR /dB	Q
Original signal	20.187	5.0011
Reconstructed signal	34.490	4.0562

4 Conclusion

A ground-penetrating radar (GPR) signal reconstruction method based on the matrix pencil (MP) method is proposed to address signal quality degradation caused by random noise. The method adopts a damped exponential signal model and reconstructs effective GPR signals by estimating key parameters such as the number of dominant poles, residues, and pole values.

Numerical simulation results show that the MP method can effectively suppress noise under different signal-to-noise ratio (SNR) conditions. The number of dominant poles (M) has a significant influence on the reconstruction: an appropriate *M* achieves optimal denoising and signal restoration, whereas an excessively large or small M induces severe waveform oscillation.

Laboratory physical model tests and full-scale shield tunnel platform experiments further verify the practicability of the proposed method. After MP processing, the high-frequency random noise in original GPR data is obviously eliminated, the waveform becomes smoother, and the image resolution is greatly improved. Quantitative indices including peak signal-to-noise ratio (PSNR) and image entropy, demon-

strate that the proposed method effectively enhance data quality while retaining weak reflection features of targets such as underground cavities and grouting defects.

This study proves that the MP method is reliable for GPR signal denoising and reconstruction. It This study demonstrates that the MP method is reliable for GPR signal denoising and reconstruction. It provides an effective technical reference for grouting quality detection, underground defect identification, and other GPR engineering applications.

References

1. Forte, E., & Pipan, M.,2017. Review of mult-offset GPR applications: Data acquisition, processing and analysis. Signal processing 132,210-220,https://doi.org/10.1016/j.sigpro.2016.04.011.
2. Kumar, B. S., Sahoo, A. K., & Maiti, S., 2021. Removal of clutter and random noise forgpr images. In 2021 IEEE 18th India Council International Conference (INDICON),Guwahati, India, 1-6,https://doi.org/10.1109/INDICON52576.2021.9691520.
3. Baili, J., Lahouar, S., Hergli, M., Amimi, A., & Besbes, K.,2006. Application of the discrete wavelet transform to denoise GPR signals. In 2nd InternationalSymposium on Communications, Control and Signal Processing, Marrakech, Morocco , 11, https://www.eurasip. org/Proceedings/Ext/ISCCSP2006/defevent/papers/cr1102.pdf.
4. Kim, J. H., Cho, S. J., & Yi, M. J, 2007. Removal of ringing noise in GPR data by signal processing. Geosciences Journal 1,75-81, https://doi.org/10.1007/BF02910382.
5. Nuzzo, L., 2003.Coherent noise attenuation in GPR data by linear and parabolic Radon Transform techniques. Annals of Geophysics 3 , 533-547, https://doi.org/10.4401/ag-3426.
6. Lahouar, S,2003. Development of data analysis algorithms for interpretation of ground-penetrating radar data. Virginia Polytechnic Institute and State University.
7. Wang, W., Du, W., Li, Y., & Jia, Z., 2025. Advanced adaptive median filter for reducing salt-and-pepper noise in GPR data. IEEE Geoscience and Remote Sensing Letters 22, 1-5, https://doi.org/10.1109/lgrs.2025.3532986.
8. Jiang, Y., Wang, H., Cai, Y,& Fu, B., 2022. Salt and pepper noise removal method based on the edge-adaptive total variation model. Frontiers in Applied Mathematics and Statistics, 8, 1-9, https://doi.org/10.3389/fams.2022.918357.
9. Zhang L., Zhang S., Ling T., & Huang, F., 2023. Biorthogonal wavelet energy entropy method with different time windows for strong interference processing of GPR signals. Journal of Applied Geophysics 216, 105158, https://doi.org/10.1016/j.jappgeo.2023.105158.
10. Liu X., Ling T., Liu W., &Jiang, Y., 2024. Accurate gain method for ground-penetrating radar signals based on stationary wavelet packet transform. Journal of Applied Geophysics 228, 105473, https://doi.org/10.1016/j.jappgeo.2024.105473.
11. Liu C, Song C, &Lu Q,2017. Random noise de-noising and direct wave eliminating based on SVD method for ground penetrating radar signals. Journal of Applied Geophysics144,125-133, https://doi.org/10.1016/j.jappgeo.2017.07.007.
12. Troiano A., &Di Giuseppe M. G., 2020. Application of principal component analysis to geo- electrical recordings. Journal of Applied Geophysics 178,104038, https://doi.org/10.1016/j.jappgeo.2020.104038.
13. Shkolnikov Y. P., 2012. Weighted principal component analysis for real-time background removal in GPR data, in Detection and Sensing of Mines, Explosive Objects, and Obscured Targets XVII. SPIE 8357,663-667, https://doi.org/10.1117/12.921116.
14. Kabourek V., Cerny P., &Mazánek M., 2012. Clutter reduction based on principal component analysis technique for hidden objects detection. Radioengineering 1,464-470.
15. Li J.H., He Z. X., Yang J., Shu J., M., Wen J.L., &Xiao Q. L., 2019. Scale and rotation statistic-based self-adaptive function for ground penetrating radar denoising in curvelet domain. Acta Phys. Sin. 9,74-83.
16. Leibowitz, C., & Weiss, A. J,2022. Underground cavity detection through group dispersion of a

GPR signal. Remote Sensing 19,4808, https://doi.org/10.3390/rs14194808.
17. Guo J., & Zhou X., 1992. Random nolse elimination using f-x domain prediction. OGP 5,655~661,https://doi.org/10.13810/j.cnki.issn.1000-7210.1992.05.011.
18. Huang Z., Cao J., &Zhou C., 2012. The high-resolution denoise processing of ground-penetrating radar data and its engineering application. Journal of Fuzhou University(Natural Science Edition) 4 ,521-526.
19. Sun B., Zhao Y., &Zhang Qi.,2007. Classifying the stratums in the images from the geology radar sonde based on the BP neutral network and median filtering. Journal of Dalian Maritime University 35, 153-156, https://doi.org/10.16411 /j.cnki.issn1006-7736.2007.s1.056.
20. Wu S., Ning X. B., &Yang T. W., 2013. Neural network-based denoising for ground- penetrating radar data. Geophysical and Geochemical Exploration 5,1298-1306.
21. Tian C., 2023. Signal Denoising of Ground-penetrating Radar Based on Depth Neural Network. Shandong Technology and Business University, https://doi.org/10.27903/d.cnki.gsdsg. 2023.000013.
22. Aqel Abueladas A. E. R., &Akawwi E, 2020.Ground penetrating radar inspection for Subsurface Historical Structures at Baptism (El-Maghtas) site, Jordan. Geoscientific Instrumentation, Methods and Data Systems Discussions 2,1-21, https://doi.org/10.5194/gi-9-491-2020.
23. Hebbache K.,Boubaya D., 2022. 2D electrical resistivity tomography (ERT) and GPR methods for soil characterization near Tiaret, northwest of Algeria-a case study. Arabian Journal of Geosciences 22,1663, https://link.springer.com/article/10.1007/ s12517-022-10956-z.
24. Valence E.,Baraer M.,Rosa E.,Barbecot F., &Monty C., 2022. Drone-based ground- penetrating radar (GPR) application to snow hydrology. The Cryosphere 9,3843,https:// doi.org/10.5194/tc-16-3843-2022.
25. Gao J.,Yuan D.,Tong Z.,& Yu D., 2020. Autonomous pavement distress detection using ground penetrating radar and region-based deep learning. Measurement 164,108077，https://doi.org/10.1016/ j.measurement.2020.108077
26. Xu J., REN Q., Huang L., 2018. GPR signal analysis method based on variational mode decomposition. Journal of Hohai University(Natural Sciences) 6,545-550, https://doi.org/ 10.3876/j.issn. 1000-1980.2018.06.012.
27. Wang X., Liu S., Cheng H., 2017. Applicatioon of Shearlet Transform for Suppressing Random Noise in GPR Data. Journal of Jilin University(Earth Science Edition) 6, 1855-1864, https://doi.org/ 10.13278/j.cnki.jjuese.201706303.
28. Zhang, X., Qin, Y., Hu, Z., Hu, X., Feng, X., & Chai, Y.2022. GPR Energy Attribute Slices Based on Multivariate Variational Mode Decomposition and Teager-Kaiser Energy Operator. Remote Sensing 19, 4805, https://doi.org/10.3390/rs14194805.
29. Shen H. Y., &LI Q. C., 2010. New idea for seismic wave filed separation and denoising by singular value decomposition(SVD).Progress in Geophys 1,225-230, https://doi.org/10.3969/ j.issn.1004-2903. 2010.01.030.
30. Xue, W., Luo, Y., Yang, Y., & Huang, Y. ,2019. Noise Suppression for GPR Data Based on SVD of Window-Length- Optimized Hankel Matrix. Sensors 17,3807, https://doi.org/10.3390/s19173807.
31. Qin Y., Huang C., Lu M.& Xu W., 2015. Adaptive clutter reduction based on wavelet transform and principal component analysis for ground penetrating radar. Journal of Radars 4,445-451.https://doi.org/10.12000/ JR15013, 2015.
32. Wang R.,Yin T.,Zhou E., &Qi B.,2022. What Indicative Information of a Subsurface Wetted Body Can Be Detected by a Ground- Penetrating Radar (GPR)? A Laboratory Study and Numerical Simulation. Remote Sensing 18,4456, https://doi.org/10.3390/ rs14184456.
33. Jing, Z., Ke, Y., Pengyue, W., Shuqi, J., & Xingzhi, T. , 2017. GPR data noise attenuation based on the Shearlet transform. Journal of Mining Science and Technology 3,228-234.
34. Shang, K., Zhang, F., Song, A., Ling, J., Xiao, J., Zhang, Z., & Qian, R.,2022. Fast Segmentation and Dynamic Monitoring of Time-Lapse 3D GPR Data Based on U-Net. Remote Sensing 17,4190, https://doi.org/10.3390/ rs14174190 .
35. Wu X., Song K., &Shi S., 2024. Research on Noise Reduction Method of GPR Based on PM Algorithm and Noise Recognition Model. Radio Engineering 10,2279-2287.

36. Wang H., Gao D., &He Y., 2024. Construction and DRDU-Net Based on Denoising Algorithm for GPR Image Dataset. Journal of Hunan University(Natural Sciences) 6,20-28, https://link.oversea.cnki.net/doi/10.16339/j.cnki.hdxbzkb. 024263.
37. Xie X., Zhai J., &Zhou B.,2021. Back-fill grouting quality evaluation of the shield tunnel using ground penetrating radar with bi-frequency back projection method. Automation in Construction 121 ,103435, https://doi.org/10.1016/j.autcon.2020.103435.
38. Mallat, S. G., & Mallat, S,1999. A wavelet tour of signal processing . San Diego: Academic press..
39. Zhou D. H., Zhou J. K., &Xia T. X., 2023. Suppression of high frequency random noise in seismic data by self-adaptive threshold of three parameter wavelet transform. Chinese J. Geophys.5, 2095-2111, https://doi.org/10.6038/cjg2022P0862.
40. Zheng J., Liu W., Ma N.,& Chen, X., 2018 Clutter reduction for gound penetrating radar signal. Electronic Measurement Technology 21, 63-66. https://doi.org/10.19651/j.cnki.emt.1802170.
41. Liu X.n, &Jia M., 2015. Identification and positioning of urban underground pipeline based on joint denoising of improved EMD and wavelet threshold. Journal of Safety Science and Technology 6,56-62.
42. Zhang Z., &Liu Y., 2017. Signal processing of ground penetrating radar based on KL transform in wavelet domain. Goal Geology and Exploration 2,70-72.
43. Zou Y., Gao X., &LI X.,2016. Multiband radar signal high precision fusion imaging method based on matrix pencil algorithm. Systems Engineering and Electronics 5,1017-1024.
44. Kang X., Qu Y., Jiao Z., Wang, D., & Ning, R.,2014. Power frequency Phasor Extraction Based on Least-square Matrix Pencil Algorithm. Automation of Electric Power Systems 21, 66-70
45. Yang Q.,Wang H., Chen C., & Zhang, Y, 2023. A fast DOA estimation method for nested MIMO radar based on matrix pencil. Modern Radar 5, 92-99.
46. Zheng K.i, Wang X., &Chen B.,2010. Reconstruction of time domain airborne electromagnetics response data based on matrix pencil method. Geophysical and Geochemical Exploration 6,737-740 .
47. Liu L., &Tan F., 2019. Research on ground penetrating radar signal denoising based on principal component analysis. Computing Techniques for Geophysical and Geochemical Exploration 5,674.
48. Sarkar T.K., &PEREIRA O., 1995.Using the matrix pencil method to estimate the parameters of sumof complex exponentials. IEEE Antennas & Propagation Magazine 1,48-55, https://doi.org/ 10.1109/74.370583.
49. Warren C., Giannopoulos A, &Giannakis I., 2016. gprMax: Open source software to simulate electromagnetic wave propagation for Ground Penetrating Radar. Computer Physics Communications 209,163-170, https://doi.org/10.1109/74.370583.
50. Hu S., Xu G., &Ma F., 2019. Experimental study on antenna spacing of ground penetrating radar detection of grouting material behind shield segment. Journal of Central South University(Science and Technology) 2,360-367.
51. Ma F., Tang F., &Huang S., 2022. GPR test and application based on shield tunnel segment grouting simulation platform. Mineral Resources and Geology 4,854-864. https://doi.org/ 10.19856/ j.cnki.issn.1001-663.2022.04.021.

Funding

This work was supported by the Key Laboratory of Geophysical Electromagnetic Probing Technologies of Ministry of Natural Resources. Award Number: KLGEPT202404.